High-throughput Single-cell CNV Detection Reveals Clonal Evolution During Hepatocellular Carcinoma Recurrence

Liang Wu[1,2,3,#,*], Yuzhou Wang[2,#], Miaomiao Jiang[2,#], Biaofeng Zhou[1,2,3], Yunfan Sun[4], Kaiqian Zhou[4], Jiarui Xie[2,3,5], Yu Zhong[2,3,5], Zhikun Zhao[2], Michael Dean[6], Yong Hou[1,2,3], Shiping Liu[1,2,3,*]

[1] *BGI Education Center, University of Chinese Academy of Sciences, Shenzhen 518083, China*

[2] *BGI-Shenzhen, Beishan Industrial Zone, Shenzhen 518083, China*

[3] *Shenzhen Key Laboratory of Single-Cell Omics, BGI-Shenzhen, Shenzhen 518100, China*

[4] *Department of Liver Surgery & Transplantation, Liver Cancer Institute, Zhongshan Hospital, Fudan University; Key Laboratory of Carcinogenesis and Cancer Invasion, Ministry of Education, Shanghai 200032, China*

[5] *School of Biology and Biological Engineering, South China University of Technology, Guangzhou 510640, China*

[6] *Laboratory of Translational Genomics, Division of Cancer Epidemiology & Genetics, National Cancer Institute, Gaithersburg, MD 20877, USA*

[#] Equal contribution.

[*] Corresponding authors.

E-mail: wuliang@genomics.cn (Wu L), liushiping@genomics.cn (Liu SP).

Abstract

Single-cell genomics provides substantial resources for dissecting cellular heterogeneity and cancer evolution, but classical DNA amplification-based methods are low-throughput and introduce coverage bias during sample preamplification. We developed a **s**ingle-**c**ell **D**NA library preparation method without **p**reamplification in **n**anolitre scale (scDPN). The method has a throughput of up to 1,800 cells per run for copy number variation (CNV) detection. Also, it has a lower level of amplification bias and noise than the multiple displacement amplification (MDA) method and showed high sensitivity and accuracy based on evaluation in cell lines and tumour tissues. We used this approach to profile the tumour clones in paired primary and relapsed tumour samples of hepatocellular carcinoma (HCC). We identified 3 clonal subpopulations with a multitude of aneuploid alterations across the genome. Furthermore, we observed that a minor clone of the primary tumour containing additional alterations in chromosomes 1q, 10q, and 14q developed into the dominant clone in the recurrent tumour, indicating clonal selection during recurrence in HCC. Overall, this approach provides a comprehensive and scalable solution to understand genome heterogeneity and evolution.

KEYWORDS: Single-cell sequencing; Hepatocellular carcinoma; Heterogeneity; Clonal evolution; Relapse

Introduction

Heterogeneity is pervasive in human cancer [1] and manifests as morphologic, transcriptomic, and genetic differences between cells. However, intercellular genetic heterogeneity in cell populations is often obscured in genome analysis at the bulk level. Single-cell technologies have advanced rapidly in the past decade and can detect variants at the single-cell level [2-4]. Technologies for transcriptome analysis have been used to profile intra-tumour heterogeneity or define immune infiltration in various cancer types [5-13]. Although less widely utilized due to throughput and cost limitations, single-cell genome sequencing is a powerful tool to track clonal dynamics and infer evolutionary trajectories [14-18].

Most strategies for single-cell whole-genome sequencing (WGS) require whole-genome amplification (WGA) before library construction, which introduces bias and increases cost. The degenerate oligonucleotide-primed PCR (DOP-PCR) method attempts to amplify the entire single-cell genome by random oligonucleotide priming [19]. However, it preferentially amplifies regions rich in cytosine and guanosine, resulting in lower genomic coverage. Multiple displacement amplification (MDA) is another commonly used avenue utilizing random primers and the high fidelity φ29 polymerase. This method generates data with good genome coverage and lower error rates. However, due to the polymerase's strand displacement activity [20], compromised uniformity is not suitable for copy number variation (CNV) detection. A hybrid method called multiple annealing and looping based amplification cycles (MALBAC) amplifies the genome with random primers and creates looped precursors to prevent continuous amplification before the PCR, achieving a better uniformity [21]. The other category of single-cell genome sequencing approaches is preamplification-free and transposase-based, including linear amplification via transposon insertion (LIANTI) [22], direct library preparation (DLP) [23], and transposon barcoded (TnBC) methods [24]. These approaches transpose single-cell genomic DNA directly and add common sequences to the end of the fragments for

further amplification, reducing biases compared with preamplification-based techniques. These methods are based on a single tube or use complicated microvalve-based microfluidic chips, limiting the throughput.

Hepatocellular carcinoma (HCC) is a high-grade malignancy with a high recurrence rate of up to approximately 60% within 5 years [25]. As a risk factor for reduced survival, early recurrence of HCC is ascribed to a residual tumour and intrahepatic micrometastasis, closely related to intra-tumour heterogeneity [26]. Next-generation sequencing (NGS) studies based on cell population have reported a high degree of intra-tumour heterogeneity in HCC [27, 28]. A single-cell triple-omics approach applied to 26 tumour cells from HCC identified 2 tumour clones based on their CNV profiles [29]. Also, monoclonal and polyclonal origins have been reported recently based on single-cell WGS of ~ 30 cells in two individual patients [30]. However, a large number of cells are required to more comprehensively understand the heterogeneity in HCC, clonal expansion, and selection during HCC relapse.

Here, we developed an unbiased preamplification-free **s**ingle-**c**ell **D**NA library **p**reparation in **n**anolitre scale (scDPN) method using microwell chips and a 72 × 72 dual indexing strategy, which is capable of processing up to ~1,800 single cells in parallel. This approach can obtain highly sensitive and accurate single-cell CNV (scCNV) profiles based on evaluations in cell lines and tumour samples. We further applied this approach to paired primary and relapsed HCC tumour samples from the same patient. We identified 3 clonal subpopulations with aneuploid alterations across the genome. Furthermore, we noticed that relapsed tumour cells were originated from a minor subpopulation of the primary tumour, indicating clonal selection during HCC recurrence.

Results

Microwell-based single-cell DNA library preparation workflow

To increase scCNV detection efficiency, we developed a preamplification-free and unbiased single-cell DNA library preparation approach called scDPN for

high-throughput scCNV detection, which provides a comprehensive, scalable solution for revealing genomic heterogeneity. The workflow of scDPN includes three main parts: cell isolation and single-cell identification, transposase-based (Tn5) library construction, and library pooling and sequencing. The first two steps were carried out in a 5,184 microwell chip (**Figure 1**). A cell suspension stained with Hoechst and propidium iodide (PI) was dispensed into the microwell chip with a MultiSample NanoDispenser (MSND). Cell suspensions with a range from 0.5 to 2.6 cells/50 nL (10~52 cells/μL) were optimum to obtain more than 1,000 wells with single-cell due to the cell counts per well followed a Poisson distribution. We used automated imaging to identify the number of cells and their viability, using fluorescent Hoechst and PI signals on a fluorescence microscope. Only microwells with single and viable cell ($Hoechst^{+}PI^{-}$) were selected for cell lysis and transposase fragmentation. Individual single-cell products were discriminated using 72 × 72 paired barcoded primers dispensed in succession with two individual dispensing steps. After several cycles of PCR, the barcodes and sequencing adaptors were added to both ends of the fragmented DNA. The microwell chip was then inverted, and all the barcoded libraries were collected into a pooled library. We determined the size distribution of pooled single-cell libraries by Agilent 2100 analysis (Figure S1). The libraries were then purified and cyclized for single-end 100 bp (SE100) sequencing on BGISEQ-500 [31].

Assessment of data quality and uniformity under different reaction conditions

The HeLa S3 and YH cell lines, HCC adjacent normal liver tissue (ANT), and tumour tissues were processed and sequenced at 0.02× depth (~600k reads under SE100). To confirm whether our approach can generate enough data for scCNV detection, we draw a CNV saturation curve using three tumour cells with deeper sequencing depths up to 0.15× (**Figure 2A**, Materials and Methods). The number of detected CNVs increased in proportion to the number of randomly extracted uniquely mapped deduplicated reads (UMDR). When the amount of UMDR reached 300k, with an

131 average sequencing depth of 0.01×, the detected CNV counts were saturated (Figure
132 2A).

133 We tested a combination of transposase (T1, T2, T3) and proteinase (P1, P2)
134 reaction conditions to optimize the protocol. Single-cell libraries with raw data above
135 30k reads (5% of average reads) were assumed to have a template-based reaction, and
136 148 cells from 5 conditions were qualified (Table S1). Afterward, we selected the
137 cells with oversaturated reads (UMDR > 300k) for further accuracy assessment. It
138 was evident that condition T2_P1 (65%) showed the highest rate of cells passing the
139 filtering criteria; conditions T1_P1, T2_P2, and T3_P2 showed a medium utilization
140 rate between 40%~50%; and T3_P1 showed the lowest utilization rate, below 30%
141 (Table S1). The qualified cells are listed in Table S2.

142 We statistically evaluated several features of these cells in different conditions,
143 including mapped reads, coverage, duplication rates, and median absolute pairwise
144 difference (MAPD) values. As the amount of sequencing reads affects these values,
145 we down-sampled each single-cell library to 400k raw reads for comparison.
146 Single-cell libraries treated with condition T3_P1 showed significantly fewer mapped
147 reads and lower coverage (Figure S2A). A low duplication ratio reflects high data
148 utilization. Conditions T2_P1, T2_P2, or T3_P2 had a mean duplication rate below
149 20%, which were lower than T1_P1 or T3_P1 (**Figure 2B**).

150 As a measurement of the bin-to-bin variation in read coverage, MAPD is an
151 indicator of the evenness of WGA. Conditions T2_P1, T3_P1, and T3_P2 exhibited
152 lower MAPD values (0.26 ± 0.07, 0.26 ± 0.03, and 0.23 ± 0.04, respectively, under 5k
153 bins) compared with condition T1_P1 (0.37 ± 0.15 under 5k bins, $P < 0.05$) (Figure
154 2B). All of these conditions showed a much lower MAPD (mean MAPD < 0.4, 0.34
155 M mapping reads under a bin size of 300 kb) than that of normal cells prepared by
156 MDA (MAPD: 0.4-0.6, 1.5 M mapped reads under a bin size of 500 kb [32]). We
157 observed that CNV profiles generated from poor quality libraries had significant noise
158 and larger MAPD values, so we set MAPD ≤ 0.45 as a cut-off for acceptable quality

according to previous reports [32]. Because aberrant chromosomes influence MAPD, we compared the utilization rates from the same HCC tumour tissue under different conditions. The results showed that T2_P1 and T2_P2 had higher utilization rates up to 100%, by using a selection criterion of MAPD ≤ 0.45 for bin sizes of 600 kb or 300 kb (Figure S2B).

To further evaluate this approach's genome-wide uniformity, we drew Lorenz curves for each condition and the data generated by the MDA method [24]. There were no substantial differences between the five conditions, and they all showed better uniformity than the MDA method (**Figure 2C**). Besides, the Lorenz curves demonstrated that scDPN had comparable uniformity with DOP-PCR, MALBAC, LIANTI, TnBC, a single-cell sequencing method that combines combinatorial indexing and linear amplification (sci-L3) [33], and the 10x genomics CNV platform (**Figure 2D**). The T2_P1 condition was chosen as optimal for further applications.

scDPN provides reliable data for accurate scCNV detection

To assess the sensitivity and accuracy of CNV calling with a depth of 300k reads, we first generated analogue data of CNVs of different sizes (1~15 Mb), with 20 variations generated for each size (Materials and Methods). Approximately 80% of CNVs above 2 Mb were detected in 5k, 10k, or 20k bins (Figure S3A). The false discovery rate (FDR) was between 0.3~0.4 when detecting CNVs of 1 Mb and decreased to below 0.25 when detecting CNVs ≥ 2 Mb using 5k bins (Figure S3B).

To assess the approach's reliability, we investigated the consistency of CNV profiles between single-cell and bulk populations. We used normal (YH) and tumour (HeLa S3) cell lines for single-cell copy number analysis and compared the results to the bulk CNVs from published HeLa S3 [34] and YH data [35]. HeLa S3 cells are known to harbour germline CNVs of defined sizes. The CNV profiles of single HeLa S3 cells were similar to the bulk data; however, this analysis did not detect a deletion on chromosome 4 posted in bulk HeLa S3 DNA (**Figure 3A** and S3C). We also observed different copy number states in chromosomes 13 and 18, which agreed with

Liu's discovery of substantial heterogeneity between HeLa variants from other laboratories [36]. The YH cells were B cells from a healthy donor, who was considered without significant CNVs. As expected, the single-cell YH cell CNV profile only had minor point CNV fluctuations (**Figure 3B** and S3C).

We then applied scDPN to an HCC tumour sample as well as paired ANT. The bulk tumour sample and peripheral blood mononuclear cells from the same patient (HCC01) were also subjected to whole-exome sequencing. We obtained 58 cells from HCC tumour tissue and 10 cells from ANT after filtering (> 300k reads, MAPD < 0.45). All 10 cells from ANT had no significant CNVs, as expected. One cell in the tumour did not have any CNVs and was considered normal (Figure S3C). The other 57 tumour cells had gain in 2p25.3-2p16.2, loss at 10q, and 56 had 8q11.23-8q24.3 gain (**Figure 3C** and S3C). This result indicated that there was only one major tumour clone in the HCC01 primary tumour. By comparing a representative copy number profile of a HCC tumour cell with a bulk CNV profile inferred from whole exome sequencing data (Materials and Methods), we observed concordant chromosome duplications of chromosomes 2, 8, and 12 and a deletion on chromosome 10, verifying the reliability of our CNV data. For example, the CNV profiles revealed multiple copy alterations, including 2p25.3-2p16.2, and 8q11.23-8q24.3, which are also present in the bulk DNA (Figure 3C).

Single-cell CNV detection reveals tumour clonal subtypes in HCC

Genetic heterogeneity in HCC has been described in somatic nucleotide variations (SNVs) by NGS or SNP array of multiple regions from the same primary HCC bulk tumour tissue [37], but there are few studies at the single-cell level. Thus, we used scDPN to investigate tumour subclones in patient HCC02. After quality control (UMDR $\geq$ 0.30 M, MAPD $\leq$ 0.45), we obtained 106 cells from the primary tumour for subsequent CNV calling. Three cells without chromosome copy number alterations were designated as normal cells. The remaining 103 cells showed two distinct CNV patterns, indicating that at least two tumour clones existed in this

primary tumour (**Figure 4A**). The major subpopulation consisted of 87 cells with high-level amplifications on chromosomes 5p15.33-q35.3, 6p25.3-q12, 7p22.3-q36.3, 8q11.1-q24.3, and 15q11.2-q26.3 and deletions on chromosomes 6q12-q27 and 8p23.3-p11.21. Deletions of chromosomes 6q and 8p and gains in 6p and 8q are known recurrent CNVs in HCC [38]. A minor subpopulation of HCC02 comprised 16/103 (15.5%) tumour cells and had additional alterations: chromosome 1q21.1-q44 gain, 10q11.21-q23.31 loss, and 14q32.2-q32.33 loss (**Figure 4B**). We also observed common alterations in chromosomes 5, 6, 7, 8, and 15 in the same patient's bulk tumour. However, the unique alterations in chromosomes 1, 10, and 14 found in the minor population of single cells were not detectable in the bulk tumour, demonstrating the capability of characterizing minor clones in single cells.

Clonal selection in HCC recurrence

A high recurrence rate is one of the risk factors contributing to the low 5-year survival rate in HCC. Understanding the clonal evolution and selection that occurs during relapse could aid in exploring the mechanism of recurrence. To investigate the correlation between the primary and recurrent tumour, we applied scDPN to the recurrent tumour from HCC02. We obtained 118 qualified cells from the recurrent tumour using the same filtering criteria. To our surprise, except for 4 normal cells without significant CNVs, the remaining 114 tumour cells had unique CNVs detected in the minor clone of the primary tumour, including 1q21.1-q44 gain, 10q11.21-q23.31, and 14q32.2-q32.33 loss (Figure S4A). This result strongly demonstrated that the minor clone in the primary tumour repopulated to be the dominant clone during relapse in this patient.

Furthermore, a hierarchical cluster analysis was conducted on CNVs in chromosomes 1, 10, and 14, revealing three subpopulations with distinct CNV patterns (**Figure 4C)**. Clone A comprised 81 primary tumour cells with no CNVs on these three chromosomes and corresponded to the major clone in the primary tumour. Both clones B and C showed similar CNVs in these three regions. Clone B was

243 composed of 17 primary tumour cells and 12 recurrent tumour cells and was
244 considered to be a transitional state of clone C. Clone C consisted of 102 relapsed
245 tumour cells and 5 primary tumour cells, indicating that the minor clone in the
246 primary tumour developed into a dominant clone during HCC relapse.

247 To determine which characteristics were associated with clone C selection during
248 recurrence, we investigated the genes located in these unique CNV regions. We found
249 several oncogenes and tumour suppressor genes described in the Catalogue Of
250 Somatic Mutations In Cancer (COSMIC) database (Table S3). Several oncogenes
251 were located in the amplification regions on chromosome 1q21.1-q44, including
252 *ABL2*, *BCL9*, *DDR2*, *FCGR2B*, *ELK4*, and *MDM4*, while several tumour suppressor
253 genes, including *PTEN*, *FAS*, and *PRF1*, were located in the loss region of
254 10q11.21-q23.31. We further validated that patients with 10q11.21-q23.31 loss or all
255 the three alterations (1q21.1-q44 gain, 10q11.21-q23.31, and 14q32.2-q32.33 loss)
256 showed lower disease or progression-free survival rate within two years in the TCGA
257 dataset for HCC (Figure S4B). However, we did not observe a significant difference
258 between patients with 1q21.1-q44 gain/14q32.2-q32.33 loss *vs.* others in disease-free
259 survival, suggesting that the loss of 10q11.21-q23.31 may make a substantial
260 contribution to tumour clone selection during relapse in HCC.

261

262 ## Discussion

263 Single-cell genomic technologies have greatly aided the analysis of the evolution
264 of cancer genomes and the study of genetic heterogeneity in cancer. However, the
265 lack of high-throughput, cost-effective single-cell WGS approaches has limited their
266 application. Here, we developed a preamplification-free, microwell-based single-cell
267 DNA library preparation approach named scDPN, which can handle up to 1,800 cells
268 per run. A fluorescence and imaging system enabled us to select a single and viable
269 cell accounting for a lower doublet rate. Through a series of experiments, we
270 determined the optimum on-chip experimental conditions for high data quality. The

strategy for constructing libraries of scDPN was similar to the DLP and TnBC approaches. Improved version of LIANTI (sci-L3) and DLP (DLP+) [39] reported recently also have increased the throughput.

Compared with MDA methods, our platform generated single-cell genome data with better uniformity and lower noise, which decreases the required sequencing depth. Low-depth single-cell genome data of the HeLa S3 and YH cell lines and tumour samples generated by scDPN showed high sensitivity (only 0.02 × depth data needed) and accuracy compared with bulk tumour analysis. The small reaction volume substantially reduced the library construction costs to $0.5 per cell. ScDPN has the advantages of amplification uniformity, throughput, and cost over existing single-cell CNV detection methods. Additionally, we evaluated the performance of CNV detection in the cell nuclei from frozen tissues (Figure S5), which extends the application to additional cell types, including neurons and retrospective studies using frozen tissues.

However, scDPN is not suitable for SNVs detection due to low genome coverage. According to Zahn's study, sequencing reads from all cells can be merged to produce a 'pseudo-bulk' genome with deep coverage accountable to an inference of SNV. Otherwise, a collection of high-depth 'clonal genomes' can be generated by combining all cells within a clone [23]. Additionally, there is a large difference in the amount of data among single-cell libraries produced from the same run due to the differential reaction efficiency during library preparation. Therefore, further condition optimization is essential to obtain uniform library products from an individual cell.

We used scDPN to identify subgroups of HCC tumour cells that were not detected in the bulk population (Figure 4A). This analysis indicates that important information is missing from bulk level-based sequencing studies. A large cohort based on scCNV in HCC may be needed to understand the genetic variance and heterogeneity more comprehensively. Understanding the clonal selection mechanisms in HCC recurrence could guide treatment and reduce relapse in HCC. Scaling our single-cell DNA

299 preparation approach with paired primary and relapsed tumour samples could address
300 essential questions concerning subclonal dynamics, such as how specific subclones
301 evolve, evade immune surveillance, and metastasize.

302 In the profiling of CNVs in paired primary tumour cells (n = 103) and relapsed
303 HCC tumour cells (n = 114), we observed a subpopulation (clone C) as the minor
304 clone (5/103, 4.8%) in the primary tumour. This minor clone had additional CNVs of
305 1q21.1-q44 gain, 10q11.21-q23.31 loss, and 14q32.2-q32.33 loss, which developed
306 into the dominant clone (102/114, 90%) in the recurrent tumour (Figure 4C). This a
307 solid evidence to support the tumour clonal selection during HCC relapse (**Figure**
308 **4D)**. We validated in TCGA data that the loss of 10q11.21-q23.31, a region
309 containing several tumour suppressor genes, is frequent in HCC and may play a
310 crucial role in tumour clone selection during relapse. A chromosome 8p deletion has
311 been correlated with HCC metastasis [40] and exists 3 clones in this tumour. The loss
312 of 6p25.3-q12 presented in all clones would result in loss of heterozygosity (LOH)
313 across the major histocompatibility complex (MHC), which is also reported to be
314 associated with cancer metastasis [41]. Immune pressure has been proposed to shape
315 the clonal evolution of metastasis [42]. However, the drivers or critical factors
316 contributing to clonal selection during recurrence or metastasis in HCC and other
317 cancers remain unclear. High-throughput single-cell omics from a large set of cancer
318 patients, may potentially address these questions and simultaneously dissect the
319 tumour environment, as well as the genetic and transcriptome characteristics of
320 tumour cells.

321

322 ## Materials and methods

323 ### Cell line and patient tissue samples

324 The lymphoblastic cell line (YH cell line) was established from an Asian genome
325 donor [35]. We purchased the HeLa S3 cell line from the American Type Culture
326 Collection (CCL-2.2, ATCC, Manassas, VA, USA). The tumour sample used for

on-chip reaction determination was a resected sample of a 45-year-old male patient (HCC01) with a primary HCC tumour. Paired primary and relapsed HCC tumour samples were obtained from a 63-year-old male patient (HCC02). Peripheral white blood cells and paired tumour sample and adjacent normal liver tissue were also obtained for bulk whole-exome sequencing or whole-genome sequencing.

Preparation of the single-cell suspension

Cell suspension of cell lines were harvested and centrifuged at 500 g for 5 min, washed by phosphate buffer solution (PBS) buffer twice, and resuspended in PBS. The resected tumour samples were processed to a single-cell suspension using the commercial Tumour Dissociation Kit (30095929, Miltenyi Biotec, Bergisch Gladbach, Germany). Briefly, fresh tumour and adjacent normal liver tissues were cut into approximately 2-4 mm pieces and transferred into the gentleMACS C Tube containing the enzyme mix. Subsequently, the suspended cells were centrifuged at 300 g for 7 min after passing through cell strainers. The suspended cells were passed through cell strainers and centrifuged at 300 g for 7 min. The cell pellets were resuspended in 90% fetal bovine serum (FBS; 10270106, ThermoFisher Scientific, Waltham, MA, USA) with 10% dimethyl sulfoxide (DMSO; D8418-50ML, Sigma-Aldrich, St. Louis, MO, USA) and collected in a freezing container for -80 °C storage.

Single-cell DNA library preparation and sequencing

We used the ReadyProbes Cell Viability Imaging Kit (R37609, ThermoFisher Scientific, Waltham, MA, USA) that contained Hoechst and PI to identify living cells. This staining process was at 37 °C for 20 min, then washed in cold 0.5× PBS twice. For cells from tumour tissue, we added fluorescent antibody CD45 (55548, BD Pharmingen™, San Jose, CA, USA) in the staining step. Based on FACS, $CD45^-$ $Hoechst^+$ PI^- cells from the single-cell suspension were sorted into single tubes for tumour cell enrichment. Counted cells were dispensed into microwells using the ICELL8 MSND (640000, Takara Bio USA, Mountain View, CA, USA) at the

concentration of 25 cells/µl in 0.5× PBS and 1× Second Diluent (640202, Takara Bio USA, Mountain View, CA, USA) into the ICELL8® 350v Chip (640019, Takara Bio USA, Mountain View, CA, USA). We used the mixed buffer of PBS and fiducial mix (640202, Takara Bio USA, Mountain View, CA, USA) as the negative control wells. The MSND precisely dispensed 50 nL volumes into the microwells. Following cell dispensing, the chip was sealed with imaging film and centrifuged for 5 min at 500 g at 4 °C, and imaged with a 4× objective using Hoechst and PI. Following imaging, 35 nL cell lysis buffer was added to each microwell (P1: 2.89 AU/L Protease K (19155, Qiagen, Germany) and 72.8 mM pH 7.5 Tris·HCl (15567027, ThermoFisher Scientific, Waltham, MA USA); P2: 8.67 AU/L Protease K and 72.8 mM pH 7.5 Tris·HCl). The sealed chip was centrifuged for 3 min at 3,000 g and room temperature, then incubated at 50 °C for 1 h, followed by 75 °C for 20 min and finally 80 °C for 5 min to inactivate the protease. The chip was centrifuged for 3 min at 3,000 g again before 50 nL Tn5 transposition mix (T1: 0.06 U/µL Tn5 transposase (1000007867, MGI, China) and 2.4× TAG buffer (1000013442, MGI, China); T2: 2.4× TAG buffer, 0.14 U/µL Tn5 transposase; T3: 2.4× TAG buffer and 0.22 U/µL Tn5 transposase) were dispensed. After sealed, the chip was centrifuged at the same condition with the last step and incubated at 55 °C for 30 min. To stop transposase activity, 31 nL 5× NT buffer (0.25% SDS solution), 1.45 nL ddH_2O, and 2.55 nL of Ad153-forward-tag (1~72) primer [1 µM] were dispensed, centrifuged and incubated for 5 min at room temperature. Another barcode primer was added to 50 nL PCR mix1 (29.6 nL 5× KAPA Fidelity Buffer, 7.69 nL 10 mM each dNTP, 5.1 nL PhoAd153 forward primer [10 µM], 5.1 nL Ad153 reverse primer [10 µM], and 2.55 nL of 72 Ad153-reverse-tag (1~72) primer [1 µM] made by KAPA HiFi HotStart PCR Kit (KK2500, Kapa Biosystems, Cape Town, South Africa). Finally, 50 nL PCR mix2 containing 21.4 nL 5× KAPA Fidelity Buffer, 5.1 nL 1 U/µL KAPA HiFi DNA polymerase, and 23.5 nL ddH_2O was dispensed. We used the following conditions to perform PCR: 72 °C for 5 min; 95 °C for 3 min; 25 cycles of 98 °C for 3 min for 20 sec, 60 °C for 15 sec, and

72 °C for 25 sec; 72 °C for 5 min; and finally 4 °C. The final extraction of PCR products was carried out by centrifuging at 3,000 g for 3 min with an extraction kit. Product purification was performed using a 1.0× Agencourt Ampure XP bead (A63881, Beckman Coulter, Indianapolis, IN, USA) to sample ratio. Following ssDNA cyclization, digestion, and PEG32 bead purification (1000005259, MGI, China), the libraries were sequenced in SE100 on the BGISEQ-500 sequencer.

Preprocessing of sequencing data

The raw reads derived from BGISEQ-500 were assessed by SOAPnuke (v1.5.6) [43] using the parameters "-Q 2 -G". Afterward, we mapped the qualified reads to the human reference genome (hg19) by Burrows-Wheeler Aligner (BWA, v0.7.16a) [44] with BWA-MEM algorithms using arguments "-t 2 -k 32 -M /path/to/ref.fa". The output SAM files were compressed and sorted by reference coordinates and then indexed with SAMtools (v1.1.19) [45]. Subsequently, uniquely mapped reads were extracted. Reads considered "PCR duplications" were removed by "samtools rmdup" from the downstream analysis.

Detection of copy number variations

We calculated the copy number of each cell with an optimized method developed by the Baslan et.al. [35, 46, 47]. Based on the coverage suggestion of 30-180 reads per window for CNV calling from Gusnanto et al., we estimated the number of bins according to the average sequencing depth (< 1 Mbp) by the R package NGSoptwin [48]. The "bin boundaries" files for 5,000 bins in hg19 that suited the read length of 100 bp were generated. After GC content normalization, DNAcopy was employed for segmentation and copy number calculation, which points to gains and losses in chromosomes.

The FASTQ files of bulk HeLa S3 were downloaded from the NCBI Sequence Read Archive repository (SRP028541). The YH dataset was available in the GigaScience repository, GigaDB (http://gigadb.org/dataset/100115) [35].

For the matched bulk WES dataset, snp-pileup from htstools was first employed for processing BAM files using parameters "/path/to/dbsnp_150.common.hg38.vcf.gz -g -q15 -Q20 -P100 -r25,0". We then used facets [49] for copy number estimation from the paired (normal/tumour) samples.

Accuracy of CNV detection from the low coverage single-cell WGS data

The accuracies of CNV calling in the paper were assessed by sensitivity and FDR gain from the simulated dataset. A series of rearranged genomes with a defined size of CNVs was randomly generated by SimulateCNVs [50]. In each of the 10 outputs, 0.1 × WGS datasets with 20 CNVs of a specific size (1, 2, 3, 5, 10, 15 Mbp) were used to randomly extract 3×10^5 uniquely mapped reads after duplicate removal with 5 replicates. A detected CNV was assumed to be true when it overlapped with at least 50% of the simulated CNVs. The sensitivity was defined as TP/(TP + FN), where the numerator was the true positive CNV mentioned above, while the total number of CNVs simulated served as the denominator. FDR was defined as FP/(FP+TP), where the numerator was the false positive CNV, and the denominator was the total number of CNVs detected by the algorithm.

Estimation of sequencing saturations

The uniquely mapped reads after duplicate removal were randomly down-sampled to 3×10^4, 6×10^4, 9×10^4, 1.2×10^5, 1.5×10^5, 1.8×10^5, 2.1×10^5, 2.4×10^5, 2.7×10^5, 3×10^5, 4.5×10^5, 6.5×10^5, 1.05×10^6, 1.5×10^6, and 2×10^6 reads. We used the down-sampled reads to estimate the sequencing saturation for our low-coverage WGS method. After calculating the copy number of each bin in the down-sampled datasets, the boundaries of the bins with copy number unequal to 2 were compared to that of samples with the highest read depth. The percentages of bins with abnormal copy number in samples with the highest coverage found in the down-sampled datasets were recorded. The saturation curves were fitted with locally weighted (LOESS) regression in geom_smooth function in the R package ggplot2 [51]. The inflection point of the curves was considered as the saturation point.

438 **Evaluation of the uniformity**

439 The FASTQ files of MDA, DOP-PCR, MALBAC, LIANTI, TnBC, and sci-L3
440 datasets were downloaded from the NCBI Sequence Read Archive repository
441 (SRR504711 for single-cell MDA, SRR1006146 for DOP-PCR, SRR975229 for
442 MALBAC, SRX2660685 for LIANTI, SRX2847396 for TnBC, SRX5179905 for
443 sci-L3) respectively. The sequence generated by 10x genomics platform was derived
444 from https://support.10xgenomics.com/single-cell-dna/datasets/1.1.0/bj_cells_1k.

445 The uniquely mapped reads after duplicate removal from all samples were
446 randomly down-sampled to 10^5 reads for uniformity evaluation. To better indicate the
447 bias of amplification methods, we binned reads into 60kb intervals across the genome
448 with an average of 20 reads per bin according to the results from Xi et al. [24]. Reads
449 in each bin were counted by bedtools2 (v2.20.1) and then applied for Lorenz model
450 estimation.

451 **CNV profiling and tumor evolution visualization**

452 MAPD is used for noise assessment in CNV calling [47, 52]. Since higher MAPD
453 values reflect the poorer quality of a cell, we excluded single-cell samples with
454 MAPD > 0.45. Segment ratios of samples were presented and clustered by hclust
455 using ‘ward.D2’. Fishplot [53] was employed for fishplot construction.

456

Ethical statements

We clarified that no animals were involved in this study. All samples involved in human beings were obtained after written informed consent and approval from the Institutional Review Board (IRB) at Fudan University ZhongShan Hospital and BGI-Shenzhen.

Data availability

The low-coverage WGS data generated by BGISEQ-500 were deposited at CNGB Nucleotide Sequence Archive (https://db.cngb.org/) with the accession ID CNP0000448 and GSA at the National Genomics Data Centre (https://bigd.big.ac.cn/) with the accession ID HRA000478 and HRA000476.

CRediT author statement

Liang Wu: Conceptualization, Methodology, Investigation, Writing-Original Draft, Writing-Review & Editing, Supervision. **Yuzhou Wang**: Methodology, Investigation, Writing-Original Draft. **Miaomiao Jiang**: Software, Data Curation, Investigation, Writing-Original Draft, Writing-Review & Editing, Visualization. **Biaofeng Zhou**: Software, Data Curation, Visualization. **Yunfan Sun**: Resources. **Kaiqian Zhou**: Resources. **Jiarui Xie**: Visualization. **Yu Zhong**: Software. **Zhikun Zhao:** Writing-Review & Editing. **Michael Dean**: Writing-Review & Editing. **Yong Hou**: Supervision, Project administration. **Shiping Liu**: Supervision, Project administration, Funding acquisition. All authors read and approved the final manuscript.

Competing interests

No conflicts of interest are declared.

Acknowledgements

This work was supported by Technology and Innovation Commission of Shenzhen Municipality (Grant No. GJHZ20180419190827179), and Science, Technology and Innovation Commission of Shenzhen Municipality (Grant No. JCYJ20170303151334808). We sincerely thank the support provided by China

National GeneBank. We thank Dr. Xiaoyun Huang for the helpful comments on the manuscript. We are also grateful to Lei Li and Shishang Qin for assistance in data analysis as well as Dandan Chen for experimental support.

Authors' ORCID IDs

0000-0001-6259-261X (Liang Wu), 0000-0003-0033-6383 (Yuzhou Wang), 0000-0002-8473-8955 (Miaomiao Jiang), 0000-0002-0261-8256 (Biaofeng Zhou), 0000-0001-9790-2761 (Yunfan Sun), 0000-0002-2763-5976 (Kaiqian Zhou), 0000-0001-9022-4881 (Jiarui Xie), 0000-0001-6902-2732 (Yu Zhong), 0000-0001-5161-7818 (Zhikun Zhao), 0000-0003-2234-0631(Michael Dean), 0000-0002-0420-0726 (Yong Hou), 0000-0003-0019-619X (Shiping Liu).

References

[1] Lawson DA, Kessenbrock K, Davis RT, Pervolarakis N, Werb Z. Tumour heterogeneity and metastasis at single-cell resolution. Nat Cell Biol 2018;20:1349-60.

[2] Macaulay IC, Voet T. Single cell genomics: advances and future perspectives. PLoS Genet 2014;10:e1004126.

[3] Shapiro E, Biezuner T, Linnarsson S. Single-cell sequencing-based technologies will revolutionize whole-organism science. Nat Rev Genet 2013;14:618-30.

[4] Gawad C, Koh W, Quake SR. Single-cell genome sequencing: current state of the science. Nat Rev Genet 2016;17:175-88.

[5] Patel AP, Tirosh I, Trombetta JJ, Shalek AK, Gillespie SM, Wakimoto H, et al. Single-cell RNA-seq highlights intratumoral heterogeneity in primary glioblastoma. Science 2014;344:1396-401.

[6] Tirosh I, Izar B, Prakadan SM, Wadsworth MH, 2nd, Treacy D, Trombetta JJ, et al. Dissecting the multicellular ecosystem of metastatic melanoma by single-cell RNA-seq. Science 2016;352:189-96.

[7] Chevrier S, Levine JH, Zanotelli VRT, Silina K, Schulz D, Bacac M, et al. An immune atlas of clear cell renal cell carcinoma. Cell 2017;169:736-49.

[8] Azizi E, Carr AJ, Plitas G, Cornish AE, Konopacki C, Prabhakaran S, et al. Single-cell map of diverse immune phenotypes in the breast tumor microenvironment. Cell 2018;174:1293-308.

[9] Lavin Y, Kobayashi S, Leader A, Amir ED, Elefant N, Bigenwald C, et al. Innate immune landscape in early lung adenocarcinoma by paired single-cell analyses. Cell 2017;169:750-65.

[10] Lambrechts D, Wauters E, Boeckx B, Aibar S, Nittner D, Burton O, et al. Phenotype molding of stromal cells in the lung tumor microenvironment. Nat Med 2018;24:1277-89.

[11] Guo X, Zhang Y, Zheng L, Zheng C, Song J, Zhang Q, et al. Global characterization of T cells in non-small-cell lung cancer by single-cell sequencing. Nat Med 2018;24:978-85.

[12] Puram SV, Tirosh I, Parikh AS, Patel AP, Yizhak K, Gillespie S, et al. Single-cell transcriptomic analysis of primary and metastatic tumor ecosystems in head and neck cancer. Cell 2017;171:1611-24.

[13] Li H, van der Leun AM, Yofe I, Lubling Y, Gelbard-Solodkin D, van Akkooi ACJ, et al. Dysfunctional CD8 T cells form a proliferative, dynamically regulated compartment within human melanoma. Cell 2019;176:775-89.

[14] Johnson BE, Mazor T, Hong C, Barnes M, Aihara K, McLean CY, et al. Mutational analysis reveals the origin and therapy-driven evolution of recurrent glioma. Science 2014;343:189-93.

[15] Wang Y, Waters J, Leung ML, Unruh A, Roh W, Shi X, et al. Clonal evolution in breast cancer revealed by single nucleus genome sequencing. Nature 2014;512:155-60.

[16] Navin N, Kendall J, Troge J, Andrews P, Rodgers L, McIndoo J, et al. Tumour evolution inferred by single-cell sequencing. Nature 2011;472:90.

[17] Hou Y, Song L, Zhu P, Zhang B, Tao Y, Xu X, et al. Single-cell exome sequencing and monoclonal evolution of a JAK2-negative myeloproliferative neoplasm. Cell 2012;148:873-85.

[18] Xu X, Hou Y, Yin X, Bao L, Tang A, Song L, et al. Single-cell exome sequencing reveals single-nucleotide mutation characteristics of a kidney tumor. Cell 2012;148:886-95.

[19] Zhang L, Cui X, Schmitt K, Hubert R, Navidi W, Arnheim N. Whole genome amplification from a single cell: implications for genetic analysis. P Natl Acad Sci USA 1992;89:5847-51.

548 [20] Spits C, Le Caignec C, De Rycke M, Van Haute L, Van Steirteghem A, Liebaers
549 I, et al. Whole-genome multiple displacement amplification from single cells. Nat
550 Protoc 2006;1:1965-70.
551 [21] Zong C, Lu S, Chapman AR, Xie XS. Genome-wide detection of
552 single-nucleotide and copy-number variations of a single human cell. Science
553 2012;338:1622-6.
554 [22] Chen C, Xing D, Tan L, Li H, Zhou G, Huang L, et al. Single-cell whole-genome
555 analyses by Linear Amplification via Transposon Insertion (LIANTI). Science
556 2017;356:189-94.
557 [23] Zahn H, Steif A, Laks E, Eirew P, VanInsberghe M, Shah SP, et al. Scalable
558 whole-genome single-cell library preparation without preamplification. Nat Methods
559 2017;14:167.
560 [24] Xi L, Belyaev A, Spurgeon S, Wang X, Gong H, Aboukhalil R, et al. New
561 library construction method for single-cell genomes. PloS one 2017;12:e0181163.
562 [25] Roayaie S, Obeidat K, Sposito C, Mariani L, Bhoori S, Pellegrinelli A, et al.
563 Resection of hepatocellular cancer </=2 cm: results from two Western centers.
564 Hepatology 2013;57:1426-35.
565 [26] Lu LC, C.-H H, Hsu C, Cheng AL. Tumor heterogeneity in hepatocellular
566 carcinoma: facing the challenges. Liver Cancer 2016;5:128-38.
567 [27] Friemel J, Rechsteiner M, Frick L, Bohm F, Struckmann K, Egger M, et al.
568 Intratumor heterogeneity in hepatocellular carcinoma. Clin Cancer Res
569 2015;21:1951-61.
570 [28] Xue R, Li R, Guo H, Guo L, Su Z, Ni X, et al. Variable intra-tumor genomic
571 heterogeneity of multiple lesions in patients with hepatocellular carcinoma.
572 Gastroenterology 2016;150:998-1008.
573 [29] Hou Y, Guo H, Cao C, Li X, Hu B, Zhu P, et al. Single-cell triple omics
574 sequencing reveals genetic, epigenetic, and transcriptomic heterogeneity in
575 hepatocellular carcinomas. Cell Res 2016;26:304-19.

576 [30] Duan M, Hao J, Cui S, Worthley DL, Zhang S, Wang Z, et al. Diverse modes of
577 clonal evolution in HBV-related hepatocellular carcinoma revealed by single-cell
578 genome sequencing. Cell Res 2018;28:359-73.
579 [31] Natarajan KN, Miao Z, Jiang M, Huang X, Zhou H, Xie J, et al. Comparative
580 analysis of sequencing technologies for single-cell transcriptomics. Genome Biol
581 2019;20:1-8.
582 [32] Garvin T, Aboukhalil R, Kendall J, Baslan T, Atwal GS, Hicks J, et al.
583 Interactive analysis and assessment of single-cell copy-number variations. Nat
584 Methods 2015;12:1058-60.
585 [33] Yin Y, Jiang Y, Lam KG, Berletch JB, Disteche CM, Noble WS, et al.
586 High-throughput single-cell sequencing with linear amplification. Mol Cell
587 2019;76:676-90.
588 [34] Adey A, Burton JN, Kitzman JO, Hiatt JB, Lewis AP, Martin BK, et al. The
589 haplotype-resolved genome and epigenome of the aneuploid HeLa cancer cell line.
590 Nature 2013;500:207-11.
591 [35] Hou Y, Wu K, Shi X, Li F, Song L, Wu H, et al. Comparison of variations
592 detection between whole-genome amplification methods used in single-cell
593 resequencing. Gigascience 2015;4:s13742-015.
594 [36] Liu Y, Mi Y, Mueller T, Mueller, T., Kreibich, S., Williams, E. G., Van Drogen,
595 A., et al. Multi-omic measurements of heterogeneity in HeLa cells across laboratories.
596 Nat Biotechnol 2019;37:314-22.
597 [37] Ling S, Hu Z, Yang Z, Yang F, Li Y, Lin P, et al. Extremely high genetic
598 diversity in a single tumor points to prevalence of non-Darwinian cell evolution. P
599 Natl Acad Sci USA 2015;112:E6496-505.
600 [38] Chen L, Chan TH, Guan XY. Chromosome 1q21 amplification and oncogenes in
601 hepatocellular carcinoma. Acta Pharmacol Sin 2010;31:1165-71.

602 [39] Laks E, McPherson A, Zahn H, Lai D, Steif A, Brimhall J, et al. Clonal
603 decomposition and DNA replication states defined by scaled single-cell genome
604 sequencing. Cell 2019;179:1207-21.
605 [40] Qin LX, Tang ZY, Sham JS, Ma ZC, Ye SL, Zhou XD, et al. The association of
606 chromosome 8p deletion and tumor metastasis in human hepatocellular carcinoma.
607 Cancer Res 1999;59:5662-5.
608 [41] McGranahan N, Rosenthal R, Hiley CT, Rowan AJ, Watkins TBK, Wilson GA,
609 et al. Allele-specific HLA loss and immune escape in lung cancer evolution. Cell
610 2017;171:1259-71.
611 [42] Angelova M, Mlecnik B, Vasaturo A, Bindea G, Fredriksen T, Lafontaine L, et
612 al. Evolution of metastases in space and time under immune selection. Cell
613 2018;175:751-65.
614 [43] Chen Y, Chen Y, Shi C, Huang Z, Zhang Y, Li S, et al. SOAPnuke: a
615 MapReduce acceleration-supported software for integrated quality control and
616 preprocessing of high-throughput sequencing data. Gigascience 2017;7:gix120.
617 [44] Li H, Durbin R. Fast and accurate short read alignment with Burrows–Wheeler
618 transform. Bioinformatics 2009;25:1754-60.
619 [45] Li H, Handsaker B, Wysoker A, Fennell T, Ruan J, Homer N, et al. The sequence
620 alignment/map format and SAMtools. Bioinformatics 2009;25:2078-9.
621 [46] Baslan T, Kendall J, Rodgers L, Cox H, Riggs M, Stepansky A, et al.
622 Genome-wide copy number analysis of single cells. Nat Protoc 2012;7:1024.
623 [47] Zhao Z, Goldin L, Liu S, Wu L, Zhou W, Lou H, et al. Evolution of multiple cell
624 clones over a 29-year period of a CLL patient. Nat Commun 2016;7:1-10.
625 [48] Gusnanto A, Taylor CC, Nafisah I, Wood HM, Rabbitts P, Berri S. Estimating
626 optimal window size for analysis of low-coverage next-generation sequence data.
627 Bioinformatics 2014;30:1823-9.

628 [49] Shen R, Seshan VE. FACETS: allele-specific copy number and clonal
629 heterogeneity analysis tool for high-throughput DNA sequencing. Nucleic Acids Res
630 2016;44:e131.
631 [50] Xing Y, Dabney AR, Li X, Casola C. SimulateCNVs: a novel software
632 application for simulating CNVs in WES and WGS data. BioRxiv 2018; 407486.
633 [51] Wickham H. ggplot2: elegant graphics for data analysis. Springer, 2016.
634 [52] Ning L, Li Z, Wang G, Hu W, Hou Q, Tong Y, et al. Quantitative assessment of
635 single-cell whole genome amplification methods for detecting copy number variation
636 using hippocampal neurons. Sci Rep 2015;5:1-3.
637 [53] Miller CA, McMichael J, Dang HX, Maher CA, Ding L, Ley TJ, et al.
638 Visualizing tumor evolution with the fishplot package for R. BMC Genomics
639 2016;17:880.
640

Figures

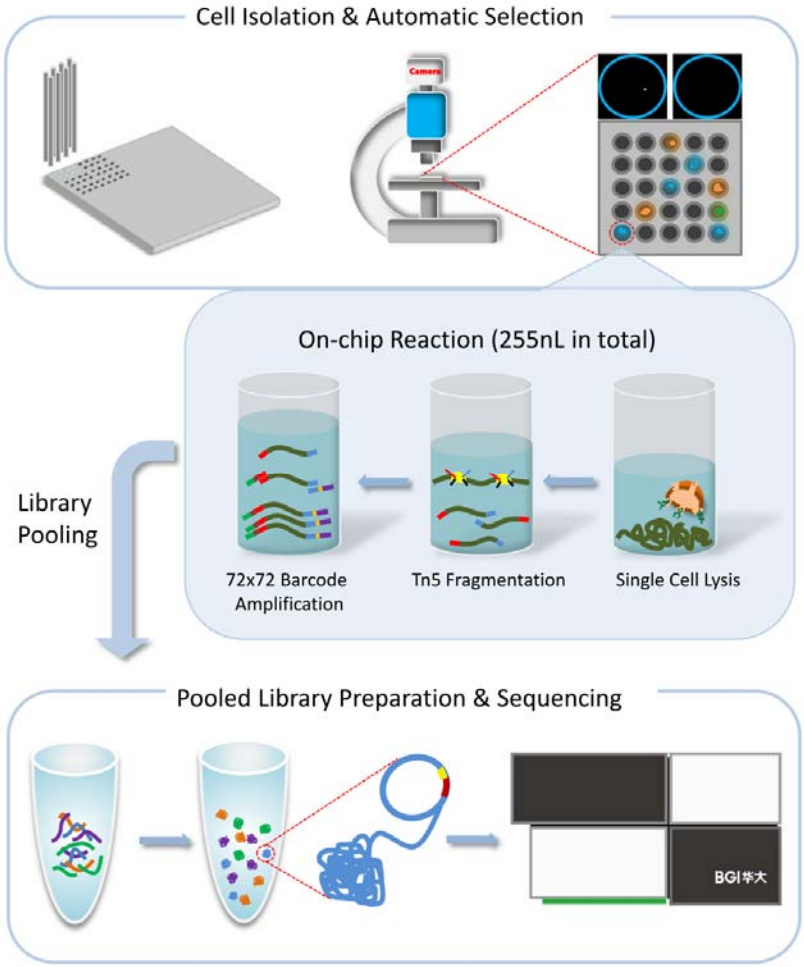

Figure 1 Schematic diagram of microwell-based single-cell genomic DNA library preparation

Stained cell suspensions were automatically dispensed into 72 × 72 microwell chips using MSND. Scanning fluorescence microscopy and cell selection software were used to discriminate wells containing single cells via the fluorescence of Hoechst and PI dyes. In the selected microwells, lysis buffer, Tn5 fragmentation buffer and 72 × 72 barcode primers were added step by step for single-cell DNA library amplification. The chip was incubated in a thermal cycler after each step. Indexed single-cell libraries were pooled by centrifugation for library purification, cyclized, and

653 sequenced on the BGISEQ500 platform. PI, propidium iodide. MSND, MultiSample
654 NanoDispenser.
655

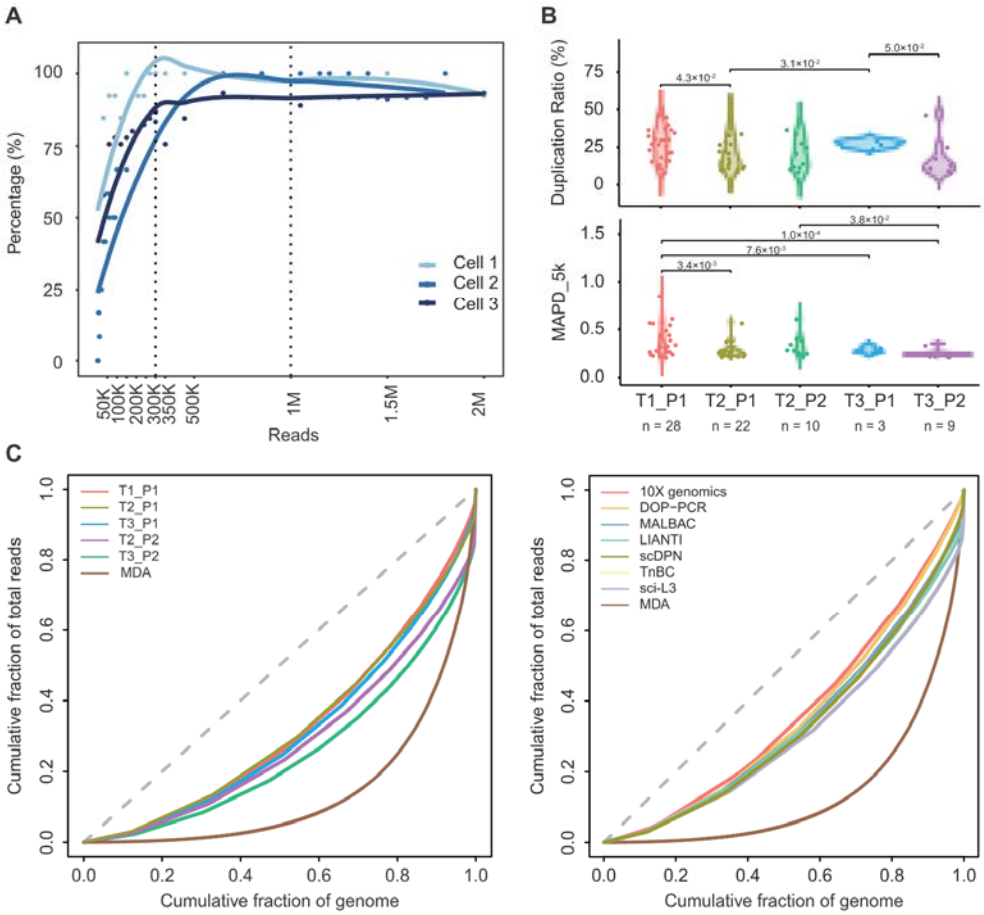

656

657 **Figure 2 Assessment of library quality under different experimental conditions**
658 **A.** CNV saturation curve. The detected CNVs increased with increasing numbers of
659 unique mapped reads. At 300k reads, the CNV counts reach saturation. **B.** Sequencing
660 data overview of 5 different single-cell lysis and transposase fragmentation conditions
661 (T1_P1, n = 28; T2_P1, n = 22; T2_P2, n = 10; T3_P1, n = 3; T3_P2, n = 9). Violin
662 charts showing the distribution of MAPD_5k and duplication ratio in different
663 conditions with 400k raw reads. The Student's T test was performed. **C**. Comparison
664 of different library preparation conditions and the MDA method using Lorenz curves
665 shows genome-wide coverage uniformity. The dotted straight black line indicates a

666 perfectly uniform genome. **D**. Comparison of different library preparation methods
667 (DOP-PCR, MALBAC, LIANTI, TnBC, sci-L3, and the 10x genomics) using Lorenz
668 curves shows genome-wide coverage uniformity. The dotted straight black line
669 indicates a perfectly uniform genome. CNV, copy number variation; MDA, multiple
670 displacement amplification; DOP-PCR, degenerate oligonucleotide-primed PCR;
671 MALBAC, multiple annealing, and looping-based amplification cycles; LIANTI,
672 linear amplification via transposon insertion; TnBC, transposon barcoded; sci-L3, a
673 single-cell sequencing method that combines combinatorial indexing and linear
674 amplification.
675

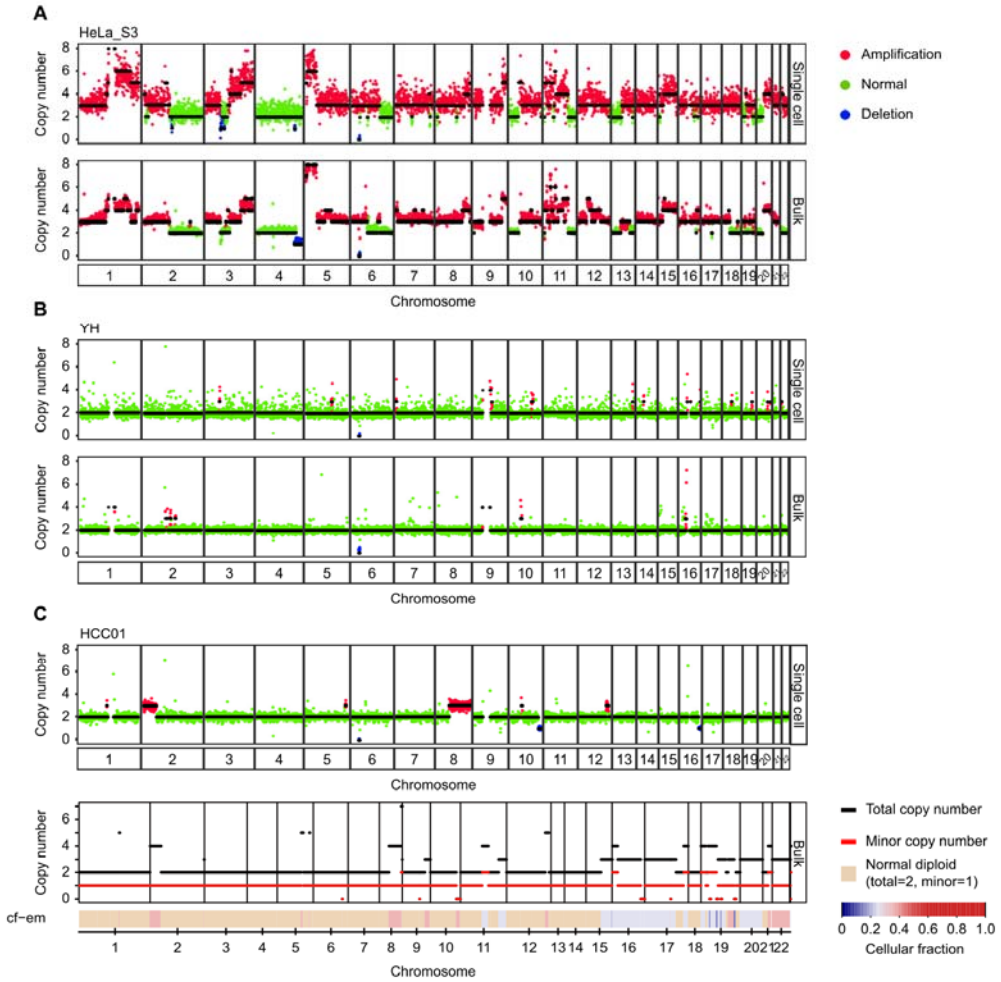

676

677 **Figure 3 scDPN provides reliable data for accurate scCNV detection**

678 **A.** Single-cell CNV profiles of HeLa S3 cells obtained using the T2_P1 condition and
679 the corresponding bulk level HeLa S3 profile from published data. **B.** Single-cell
680 resolution CNV profiles of the YH cell line obtained from the T2_P1 condition and
681 the corresponding bulk level YH profile from published data. **C.** Representative single
682 tumour cell copy number profile and corresponding bulk tumour CNV profile from
683 FACETS analysis of whole-exome sequencing data in HCC01. The second panel
684 plots the corresponding integer (total, minor) copy number calls. The estimated
685 cellular fraction profile is plotted at the bottom, revealing both clonal and sub-clonal
686 copy number events. HCC, hepatocellular carcinoma.
687

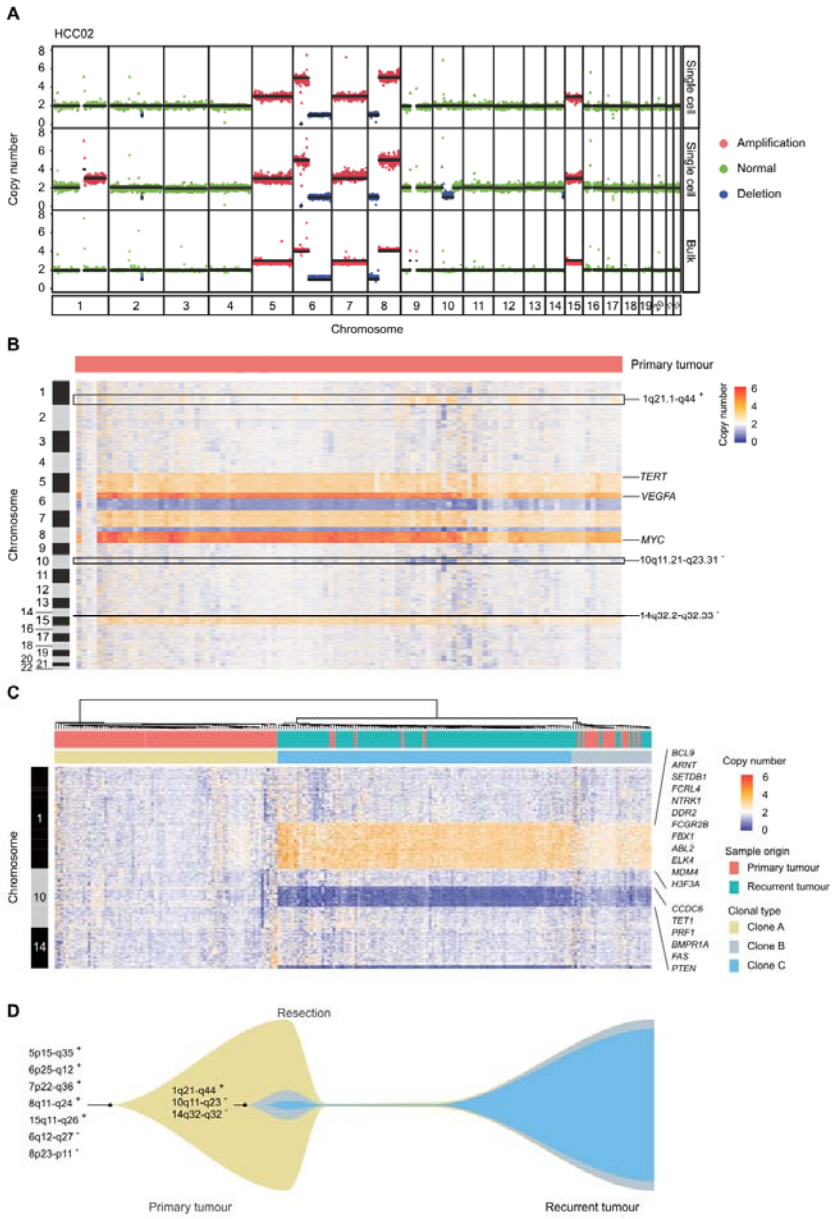

688

689 **Figure 4 Single-cell CNV profiles reveal tumour clonal selection during HCC**

690 **recurrence**

691 **A.** Two CNV patterns observed in single-cell and CNV profiles detected by bulk

692 WGS of the primary tumour in HCC02. Colours correspond to inferred copy-number

693 states; black lines indicate segment medians. **B.** Heatmap showing the copy number

694 states of all 106 cells from the primary tumour. Columns correspond to cells, and

695 rows correspond to a ~600 kb genomic bin for each chromosome. Reported

696 HCC-related genes *TERT*, *VEGFA*, and *MYC* are indicated. **C.** Heatmap showing the

697 unsupervised clustering of all tumour cells from primary (n = 103) and relapsed
698 tumours (n = 114) based on the CNVs on chr 1, 10, and 14. **D.** Schematic diagram of
699 HCC tumour clonal selection during recurrence in patient HCC02.
700

Supplementary materials

Figure S1 Quality control of the library construction

The length distribution of the library was determined using an Agilent 2100 bioanalyzer.

Figure S2 Assessment for scDNP under different conditions

A. Boxplots showing the distribution of mapped reads and genome coverage, in different conditions. The Student's T test was performed. **B**. The proportions of HCC cells (UMDR > 300K) sampled from the same patient with MAPD ≤/> 0.45 in different numbers of bins among various lysis and transposase fragmentation conditions (T1_P1, n = 22; T2_P1, n = 15; T2_P2, n = 5; T3_P1, n = 2, excluded; T3_P2, n = 4).

Figure S3 scDPN provides reliable data for accurate scCNV detection

Sensitivities (**A**) and FDRs (**B**) of the CNV detection algorithm at defined resolutions. The points and error bars represent the means and standard deviations, respectively. FDR, false discovery rate. **C**. Single-cell CNVs of different samples using low coverage. Heatmap showing the CNV profiling of HeLa S3 cells (red), YH cells (yellow), cells from adjacent liver tissue (blue), and tumour tissue (green) of HCC01. Columns correspond to cells, and rows correspond to 600 kb genomic bins for each chromosome. FDR, the false discovery rate.

Figure S4 Tumour clonal selection during HCC recurrence

A. Single-cell CNV profiling of HCC02 recurrent tumour samples. Heatmap showing the CNV profiles of all 118 cells from relapsed tumours. Columns correspond to cells, and rows correspond to 600 kb genomic bins for each chromosome. **B-C**. Kaplan-Meier analysis showing the disease/progression-free survival for patients with chr10q11.21-q23.31 deletion (**B**) and the three alterations (**C**) in the TCGA dataset for HCC.

Figure S5 Evaluation of our CNV detection method with cell nuclei

728 The distribution of mapped reads, used reads, genome coverage, and MAPD_5k of
729 either the nucleus or cells are shown by box plots, and dots indicate individual
730 samples. The Student's T test was performed.

731 **Table S1 Statistics of cells used in the adjustment of reaction parameters**

732 **Table S2 Single-cell resource for scDPN assessment and tumour clone analyse**

733 **Table S3 Oncogenes and tumour suppressor genes with copy number**
734 **alterations in our study**

735